Atomic structure of misfit dislocations in nonpolar ZnO/Al_2O_3 heterostructures

H. Zhou,[1,2,a)] M. F. Chisholm,[2] P. Pant,[1] H. J. Chang,[2] J. Gazquez,[2] S. J. Pennycook,[2] and J. Narayan[1]
[1]*Department of Materials Science and Engineering, North Carolina State University, Raleigh, North Carolina 27695, USA*
[2]*Materials Science and Technology Division, Oak Ridge National Laboratory, Oak Ridge, Tennessee 37831, USA*

(Received 13 May 2010; accepted 25 August 2010; published online 22 September 2010)

Understanding dislocation core structures at the atomic level is of significant theoretical and technological importance because of the role dislocations play in the electronic/optical properties of materials. In this paper, we report our aberration-corrected scanning transmission electron microscopy study on misfit dislocation core structures at non-polar $(11\bar{2}0)ZnO/(1\bar{1}02)Al_2O_3$ (a-ZnO/r-Al_2O_3) interface. The atomic configuration of the core structure is found to be closely related to the preferred interfacial bonding configuration. A significant number of these misfit dislocations have undergone a core structure modification involving the incorporation of Zn in the Al_2O_3 side of the dislocation. © *2010 American Institute of Physics*. [doi:10.1063/1.3489687]

With a direct band gap of 3.32 eV as well as a large exciton binding energy of 60 meV (the largest among conventional semiconductors), ZnO is one of the most attractive candidates for a host of optical devices, with applications including light emitting diodes (LEDs) and optical sensors, owing to its potential of high operating efficiency at high temperatures. Most of the reported work has focused on polar ZnO grown on c-Al_2O_3 [the (0001) plane]. However, polar heterostructures experience strong spontaneous and piezoelectric polarization fields, which reduce the overlap between the electron and hole wave functions and thus reduce the internal quantum efficiency of LEDs.[1–8] It has been shown that the growth of nonpolar films, such as GaN/(Al,Ga)N on tetragonal $LiAlO_2$ (Ref. 7) and a-plane ZnMgO/ZnO on r-plane sapphire [$(11\bar{2}0)$ZnO on $(1\bar{1}02)Al_2O_3$],[8] eliminates the polarization effects and in turn increase the quantum efficiency of LEDs. The growth of a-ZnO on r-Al_2O_3 has anisotropic lattice misfit, ranging from 18.3% [along $[01\bar{1}0]ZnO//[2\bar{1}\bar{1}0]Al_2O_3$] to 1.5% [along $[0001]ZnO//[\bar{1}101]Al_2O_3$].[9–14] The large lattice misfit has been shown to relax fully during the initial stages of growth by incorporating a network of misfit dislocations.[12–17] Previous studies have focused on the nature of the relaxation of lattice misfit strains using x-ray diffraction and high-resolution transmission electron microscopy studies.[12–14,16,17] However, the detailed atomic structure of dislocations at the interfaces has not been explored. Such study is essential since dislocations as well as the additional structural modifications that are associated with them alter the density of states, providing traps or recombination centers for electrons and holes, thereby directly affecting the electronic/optical properties of the system. In this paper, we report misfit dislocation core structures at the $(11\bar{2}0)ZnO/(1\bar{1}02)Al_2O_3$ (a-ZnO/r-Al_2O_3) interface obtained using aberration-corrected scanning transmission electron microscopy (STEM).

A dedicated VG Microscopes HB 603U scanning transmission electron microscope equipped with Nion aberration corrector operating at 300 KV accelerating voltage was employed for image acquisition and a Nion UltraSTEM operating at 100 kV was used for electron energy loss spectroscopy (EELS). The aberration corrector improved the spatial resolution of the microscope to 0.78 Å, and therefore permits direct imaging of the interface atomic structure.[18–20] ZnO films were grown by pulsed laser deposition under optimized conditions as reported earlier.[13,14] Based on the epitaxial orientation relationship determined in earlier studies: $(11\bar{2}0)ZnO//(1\bar{1}02)$ with $[0001]ZnO//[\bar{1}101]Al_2O_3$,[13,14] cross sectional STEM samples along two in-plane orthogonal zone axes ZnO [0001] and $ZnO[01\bar{1}0]$ were prepared by standard mechanical polishing and ion milling for interface study. This paper focuses on the misfit dislocations viewed along the ZnO [0001] zone axis, where the large lattice misfit of 18.3% is accommodated, and many dislocation cores show a modified core structure that reduces the strain field in the ZnO.

Figure 1(a) shows a typical view of the a-ZnO/r-Al_2O_3 interface along $ZnO[0001]/Al_2O_3[\bar{1}101]$ zone axis. As indicated by arrows, misfit dislocations, characterized by an extended strained region on the ZnO side of the interface, are found to be closely spaced and distributed on the interface, consistent with the large lattice misfit (18.3%) along the $ZnO[01\bar{1}0]//[2\bar{1}\bar{1}0]Al_2O_3$ direction. The defective area resulting from the large lattice misfit is seen well confined inside/around the dislocation cores within 3–4 monolayers and no threading dislocations were observed originating from any misfit dislocations in the studied areas. Figure 1(b) is a magnified image of a region between dislocation cores. As illustrated by the ball and stick model, the bright columns in the upper part of the image contain alternating Zn and O atoms, bonded with each other forming the hexagonal features expected when viewed along the [0001] ZnO direction.

a)Electronic mail: hzhou4@ncsu.edu.

 © 2010 American Institute of Physics

Downloaded 14 Feb 2011 to 128.219.49.9. Redistribution subject to AIP license or copyright; see http://apl.aip.org/about/rights_and_permissions

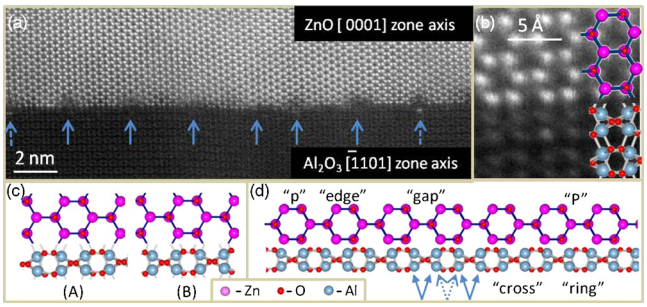

FIG. 1. (Color online) (a) STEM-Z contrast image of the $(11\bar{2}0)ZnO/(1\bar{1}02)Al_2O_3$ interface along the $ZnO[0001]/Al_2O_3[\bar{1}101]$ zone axis. Misfit dislocations, indicated by arrows, are characterized by an extended strained region (seen dark in the image) on the ZnO side of the interface. (b) Higher magnification Z contrast image of the interface between two misfit dislocation cores showing the preferred interfacial bonding configuration. (c) Schematic illustration of the two possible interfacial bonding configurations. Configuration (A), where the ZnO hexagon edge is bonded with a Al_2O_3 cross, is expected to be energetically more favorable than configuration (B), where the ZnO hexagon edge is bonded with the Al_2O_3 ring, owing to the reduced bond distortion required. (d) Schematic diagram of the interface drawn in proportion to the bulk lattice constants of the two materials, with both ends in the preferred bonding configuration (ZnO hexagon edge—Al_2O_3 cross or ZnO gap—Al_2O_3 ring, indicated by P). Pairs of arrows point to the possible locations of the dislocation line, i.e., two extra Al_2O_3 planes. Dashed arrows point to the location where broken ZnO bonds would be required.

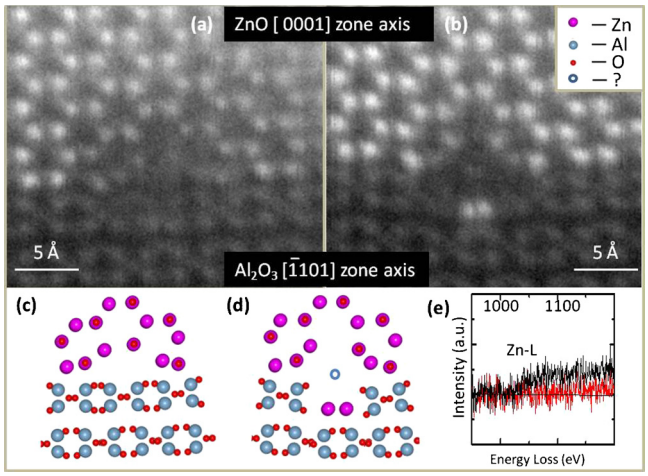

FIG. 2. (Color online) Atomic resolution Z contrast image of the most frequently observed misfit dislocation core structure (a) along with its deduced model (c). The Burgers vector of the dislocation is determined to be $1/3\langle 2\bar{1}\bar{1}0\rangle Al_2O_3$. Atomic resolution Z contrast image of a modified misfit dislocation core structure involving replacing Al atoms in the core region by Zn (b) and deduced model (d). The tensile strain in the core region is reduced, compared with that in unmodified core, as deduced from the reduced extent of strain contrast (columns with reduced intensity) seen in the image. An EELS spectrum acquired on the bright columns (the upper curve), where Zn replaces Al at the Al_2O_3 side of the dislocation core, compared with the one acquired outside the core region (the lower curve) is shown in (e). Though noisy, a Zn *L* edge is clearly present on the former. The quantification routine in digital micrograph gives difference in counts with $3.77e+004 \pm 601$ in the former compared with $0.00e+000 \pm 554$ in the latter with an integration window of 1020–1120 eV.

The less bright columns in the lower part of the image are Al columns bonded with O columns (barely visible), forming chains consisting of alternating "ring" and "cross" features, consistent with the atomic configuration expected for the $[\bar{1}101]$ projection of Al_2O_3. Figure 1(b) also provides information on the preferred interfacial bonding configuration. Our images show that the edge of the hexagonal features seen in ZnO sits directly above the cross feature in Al_2O_3. This interfacial bonding arrangement agrees well with what would be expected from simple consideration of preferred bond lengths and bond angles. As illustrated in the ball and stick model in Fig. 1(c) (drawn in proportion to the bulk lattice constants of the two materials), Al–O bonds and Zn–O bonds at the interface in configuration (A) are better able to maintain their bulk directions and lengths compared to the other configuration (B), leading to a smaller interfacial energy. As demonstrated later in this paper, this preferred interfacial bonding configuration plays an important role in misfit dislocation core structure formation.

Using this information, a schematic diagram of the unbonded interface, drawn in proportion to the bulk lattice constants of the two materials, is shown in Fig. 1(d). It is seen that Zn/O columns are not evenly distributed on the interface: pairs of closely spaced columns (forming hexagon edges) are separated by gaps at a distance equal to the largest diagonal of the hexagonal features. In contrast, Al columns are evenly distributed, however, they are not equivalent due to the asymmetric oxygen bonding environment. We distinguish pairs of Zn/O columns with "hexagon edge" versus "gap," and pairs of Al columns with "ring" versus "cross" as indicated in the diagram. When a hexagonal ZnO feature is set in its preferred location above the Al_2O_3 cross feature (indicated by the left hand "P"), it can be seen that moving along the interface the next closest perfect fit occurs between five and six $(1\bar{1}00)_{ZnO}$ spacings [six and seven $(11\bar{2}0)_{Al_2O_3}$ spacings] away, with a ZnO gap over an Al_2O_3 ring, indicated by the right hand P. It is obvious that between these regions of perfect fit, the ZnO edge features will have to move relatively large distances to be aligned with the Al_2O_3 cross features. Halfway between the regions of perfect fit, there is one ZnO edge feature and two Al_2O_3 cross features, necessitating the introduction of a misfit dislocation.

There are three possible locations for the dislocation: either beneath ZnO hexagon edge or beneath one of the two ZnO gaps on either side of the ring feature, as indicated by arrows in Fig. 1(d). The dislocations are rarely observed to be centered on the edge feature. In fact, the few dislocations with this arrangement appear wider on the ZnO side of the interface and are more likely the result of a dislocation that jogs between the two preferred gap locations along the viewing direction. Most of the misfit dislocations are seen to be centered on the ZnO gap feature, as presented in Fig. 2, suggesting that this structure is energetically more stable. This is most likely due to the fact the atomic configuration in this core structure nearly preserves the bulk ZnO configuration (no broken Zn–O bonds involved).

In a significant number of dislocations [two in Fig. 1(a) indicated by dashed arrows], bright columns are found at the Al_2O_3 side of the interface. This phenomenon is consistently seen over the entire interface on different samples. Column by column EELS (Refs. 18–20) indicates that these bright columns contain Zn. A magnified image of this type of core structure is shown in Fig. 2(b) with Fig. 2(e) showing an EELS spectrum acquired on the bright columns in comparison with that acquired on the neighboring columns outside the core. It is clear that while Zn is detected on these bright columns inside the misfit dislocation core, it is not present outside these cores. The core is modified not only chemically

Downloaded 14 Feb 2011 to 128.219.49.9. Redistribution subject to AIP license or copyright; see http://apl.aip.org/about/rights_and_permissions

but also structurally. While the Al_2O_3 lattice in the unmodified cores [Fig. 2(a)] remains almost bulklike up to the interface, in the modified cores, the Al columns at the ends of the extra Al_2O_3 planes in the dislocation are fully or partially removed and replaced by Zn, and as a result, the intensity of these columns is significantly enhanced. This modified core structure seems to be more compact, i.e., the strained/distorted ZnO region is confined in a smaller region with respect to that around dislocations with the unmodified core structure, as deduced from the extent of strain contrast (column intensities) seen in the images. This suggests the modification leads to a certain degree of strain relief in ZnO, although at the expense of the "integrity" of the Al_2O_3 lattice near the interface. The lateral tensile strain relief in ZnO mainly comes from the displacement of the Al_2O_3 lattice surrounding the missing Al columns, i.e., tilted a few degrees inward, in response to the compression strain induced by missing Al columns. Indeed, the core structure model deduced from the images shows that bonding between ZnO "edge" and Al_2O_3 cross features is maintained better in this modified core [Fig. 2(b)] than in the unmodified one [Fig. 2(a)] owing to this tilting. The Zn substitution for Al should be a result of core structure stabilization. However, considering the large local compressive strain, Zn occupation of Al sites is unexpected since Zn has a larger ionic radius. We speculate this can be attributed to the lower valence of Zn (2+ with respect to 3+ of Al). A lower valence means fewer oxygen ions are required for bonding, and as a result, the complete Zn-modified cation/anion "molecule" is smaller than the Al/O molecule it replaces. This is consistent with the observation of reduced strain seen at these chemically modified cores. On the top of the pair of "Zn" columns, a spot with weak and nonuniform intensity indicates there is one or a pair of closely spaced columns, whose composition cannot be identified, yet whose function should be the same as the pair of Zn columns beneath, i.e., to stabilize the Al_2O_3 lattice inside the misfit dislocation core. Indeed, with a different valence, the Zn occupation might stabilize the core structure not only mechanically by relieving this compression strain but also electronically by reducing the number of dangling bonds generated by missing Al columns. This core structure modification is apparently driven by strain relief, and therefore energetically favorable. However, the fact that it is not taking place in all misfit dislocations suggests that this modification is conditional, requiring diffusion of Zn to the Al_2O_3 side of the dislocation core and the diffusion of Al away from the core. The core structures may also be nonstoichiometric, as found in other oxides,[21,22] which would further influence the local electronic and optical properties. Further experimental study and theoretical calculations are needed for a complete understanding.

In summary, with the help of the aberration-corrected STEM, we were able to directly image the misfit dislocation core structures at the atomic level on the $(11\bar{2}0)ZnO/(1\bar{1}02)Al_2O_3$ (a-ZnO/r-Al_2O_3) interface along the $ZnO[0001]/[\bar{1}101]Al_2O_3$ zone axis. The dislocations are found to be perfect edge dislocations with a Burgers vector of $b=1/3\langle 2\bar{1}\bar{1}0\rangle Al_2O_3$. The atomic configuration of the core structure is closely related to the preferred interfacial bonding configuration, which is consistent with what would be expected from simple consideration of interface total energy minimization. A core structure modification involving Zn substitution for Al is observed in many of the misfit dislocations. This modification, while locally disrupting the Al_2O_3 lattice at the interface, seems to be effective in reducing the strain in the core region.

This research was supported by the National Science Foundation (NSF DMR-0803663) and DOE Office of Science, Materials Sciences and Engineering Division. H.Z. acknowledges Dr. J. He for useful discussions. Schematic drawings presented in this paper were produced using *Vesta*.[23]

[1] M. Leroux, N. Grandjean, M. Laügt, J. Massies, B. Gil, P. Lefebvre, and P. Bigenwald, Phys. Rev. B **58**, R13371 (1998).
[2] F. Bernardini, V. Fiorentini, and D. Vanderbilt, Phys. Rev. B **56**, R10024 (1997).
[3] T. Makino, A. Ohtomo, C. H. Chia, Y. Segawa, H. Koinuma, and K. Kawasaki, Physica E (Amsterdam) **21**, 671 (2004).
[4] C. Morhain, T. Bretagnon, P. Lefebvre, X. Tang, P. Valvin, T. Guillet, B. Gil, T. Taliercio, M. Teisseire-Doninelli, B. Vinter, and C. Deparis, Phys. Rev. B **72**, 241305 (2005).
[5] S. H. Park and D. Ahn, Appl. Phys. Lett. **87**, 253509 (2005).
[6] B. P. Zhang, B. L. Liu, J. Z. Yu, Q. M. Wang, C. Y. Liu, Y. C. Liu, and Y. Segawa, Appl. Phys. Lett. **90**, 132113 (2007).
[7] P. Waltereit, O. Brandt, A. Trampert, H. T. Grahn, J. Menniger, M. Ramsteiner, M. Reiche, and K. H. Ploog, Nature (London) **406**, 865 (2000).
[8] J. M. Chauveau, M. Laugt, P. Vennegues, M. Teisseire, B. Lo, C. Deparis, C. Morhain, and B. Vinter, Semicond. Sci. Technol. **23**, 035005 (2008).
[9] Y. S. Nam, S. W. Lee, K. S. Baek, S. K. Chang, J.-H. Song, S. K. Han S.-K. Hong, and T. Yao, Appl. Phys. Lett. **92**, 201907 (2008).
[10] C. C. Kuo, W.-R. Liu, W. F. Hsieh, C.-H. Hsu, H. C. Hsu, and L. C. Chen, Appl. Phys. Lett. **95**, 011905 (2009).
[11] G. Saraf, Y. Lu, and T. Siegrist, Appl. Phys. Lett. **93**, 041903 (2008).
[12] J. M. Chauveau P Venne guès, M. Laugt, C. Deparis, J. Zuniga-Perez, and C. Morhain, J. Appl. Phys. **104**, 073535 (2008).
[13] P. Pant, J. D. Budai, R. Aggarwal, R. J. Narayan, and J. Narayan, Acta Mater. **57**, 4426 (2009).
[14] P. Pant, J. D. Budai, and J. Narayan, Acta Mater. **58**, 1097 (2010).
[15] J. Narayan and B. C. Larson, J. Appl. Phys. **93**, 278 (2003).
[16] J. W. Lee, S. K. Han, S.-K. Hong, J. Y. Lee, and T. Yao, J. Cryst. Growth **310**, 4102 (2008).
[17] C. M. Wang, L. V. Saraf, and Y. Qiang, Thin Solid Films **516**, 8337 (2008).
[18] S. J. Pennycook and L. A. Boatner, Nature (London) **336**, 565 (1988).
[19] S. J. Pennycook, A. Rev. Mater. Sci. **22**, 171 (1992).
[20] P. D. Nellist, M. F. Chisholm, N. Dellby, O. L. Krivanek, M. F. Murfitt, Z. S. Szilagyi, A. R. Lupini, A. Borisevich, W. H. Sides, Jr., and S. J. Pennycook, Science **305**, 1741 (2004).
[21] M. Kim, G. Duscher, N. D. Browning, K. Sohlberg, S. T. Pantelides, and S. J. Pennycook, Phys. Rev. Lett. **86**, 4056 (2001).
[22] R. F. Klie, J. P. Buban, M. Varela, A. Franceschetti, C. Jooss, Y. Zhu, N. D. Browning, S. T. Pantelides, and S. J. Pennycook, Nature (London) **435**, 475 (2005).
[23] K. Momma and F. Izumi, J. Appl. Crystallogr. **41**, 653 (2000).

Downloaded 14 Feb 2011 to 128.219.49.9. Redistribution subject to AIP license or copyright; see http://apl.aip.org/about/rights_and_permissions